

Specific heat of stage-2 MnCl_2 graphite intercalation compound: co-existence of spin glass phase and incommensurate short-range spin order

Masatsugu Suzuki* and Itsuko S. Suzuki†

Department of Physics, State University of New York at Binghamton, Binghamton, New York 13902-6016

Tadashi Adachi and Yoji Koike

Department of Applied Physics, Graduate School of Engineering, Tohoku University, Sendai 980-8579, JAPAN

(Dated: November 2, 2021)

Stage-2 MnCl_2 GIC magnetically behaves like a quasi 2D XY antiferromagnet on the triangular lattice (in-plane lattice constant of Mn layer is 3.692 \AA and the c axis repeat distance is 12.80 \AA). The temperature (T) dependence of the zero-field cooled (ZFC) and field-cooled (FC) magnetizations shows a typical spin glass behavior below the spin freezing temperature T_{SG} ($= 1.1 \text{ K}$). The AC magnetic susceptibility shows a peak at $T = T_{SG}$ at $H = 0$. This peak shifts to the low temperature side with increasing H , according to the de Almeida-Thouless critical line. We have undertaken an extensive study on the T dependence of specific heat in the absence of an external field H and in the presence of H along the c plane. The magnetic specific heat C_{mag} at $H = 0$ shows no anomaly at T_{SG} , but exhibits double broad peaks around 5 K and 41 K . The anomaly at 41 K is the onset of short range spin correlation. The anisotropy of the DC magnetic susceptibility starts to become appreciable below 50 K . The magnetic specific heat C_{mag} at $H = 0$ is described by $C_{mag} \propto (1/T^2) \exp(-\Delta/T)$ with $\Delta = 1.41 \pm 0.03 \text{ K}$, while C_{mag} at $H = 10 \text{ kOe}$ is proportional to T . The entropy due to the broad peak around 5 K is $1/3$ of the total entropy. The residual entropy is 63% of the total entropy because of highly frustrated nature of the system. The magnetic neutron scattering indicates that a short range spin order associated with the incommensurate wave vector $|\mathbf{Q}_{incomm}|$ ($= 0.522 \text{ \AA}^{-1}$ at 0.45 K) appears below 5 K and remains unchanged down to 63 mK . The in-plane spin correlation length is only 18 \AA at 0.45 K . The low temperature phase below T_{SG} is a kind of reentrant spin glass phase where the spin glass phase coexists with a short range spin order associated with $|\mathbf{Q}_{incomm}|$.

PACS numbers: 75.40.Cx, 75.50.Lk, 75.50.Ee

I. INTRODUCTION

In stage-2 MnCl_2 GIC, the MnCl_2 layer consists of a three-layer sandwich of Cl-Mn-Cl layers, with the same layered structure as pristine MnCl_2 . The MnCl_2 layers are separated periodically by two graphite layers in stacks along the c axis. The c -axis repeat distance is 12.80 \AA . The MnCl_2 layer forms a triangular lattice (lattice constant 3.692 \AA) translationally incommensurate with the graphite host but rotationally locked into 30° with respect to it. Stage-2 MnCl_2 GIC is a suitable prototype for studying the classical two-dimensional (2D) XY -like antiferromagnet on a triangular lattice (AFT). The interplanar interaction between adjacent MnCl_2 layers, J' can be greatly reduced by these intervening graphite layers, while the antiferromagnetic intraplanar exchange interaction between Mn^{2+} spins, J_1 , remains virtually unchanged.^{1,2,3,4,5,6,7,8,9,10}

The 2D XY -like AFT has received attention from theorists because the spins in it are fully frustrated. The ground state consists of spins on three sublattices forming 120° angles with respect to each other, the $\sqrt{3} \times \sqrt{3}$ spin structure. Because there are two senses to the spin helicity, the ground state has a twofold discrete degeneracy as well as an XY -like continuous degeneracy. Consequently, it is predicted to undergo two phase transitions, one associated with Ising-type symmetry breaking and the other

with a Kosterlitz-Thouless (KT) mechanism.^{11,12,13} Note that our system has an incommensurate spin structure close to $2\sqrt{3} \times 2\sqrt{3}$ spin structure (see later). In this sense our system is different from an ideal 2D XY antiferromagnet on the triangular lattice.

The magnetic properties of stage-2 MnCl_2 GIC have been extensively studied by DC susceptibility,⁵ the zero-field cooled (ZFC) and field-cooled (FC) magnetization,⁶ AC magnetic susceptibility,^{3,4} electron spin resonance (ESR),^{2,7} specific heat,⁶ and magnetic neutron scattering.^{8,9,10} The low temperature phase below T_{SG} ($= 1.1 \text{ K}$) is a spin glass phase, reflecting the fully frustrated nature of the system. A short range spin order related to the incommensurate spin structure (typically 18 \AA in-plane spin correlation length) appears below 5 K , and remains unchanged even below T_{SG} .

In the present paper, we report the result of specific heat measurement of stage-2 MnCl_2 GIC between 0.45 K and 50 K , with and without an external magnetic field applied along the c plane. We show that the magnetic specific heat shows no anomaly at T_{SG} , but exhibits a broad peak around 5 K . It also shows a broad peak around 41 K , which is the onset of short range spin correlation. There is a relatively large residual entropy at $T = 0 \text{ K}$ reflecting the fully frustrated nature of the system. The results of specific heat measurements will be discussed in light of the experimental results of the ZFC and FC magnetization, AC magnetic susceptibility, magnetic neutron

scattering, ESR, and DC magnetic susceptibility. To this end, the previous data are extensively re-analyzed. Finally we will discuss the origin of the short range spin order related to the incommensurate spin structure. This structure is close to the commensurate structure with the periodicity of $(2\sqrt{3} \times 2\sqrt{3})$.

Recently the magnetic properties of 2D antiferromagnet on the triangular lattice, NiGa_2S_4 ($S = 1$ for Ni^{2+}) have been extensively studied.^{14,15,16} There are several features which is common to stage-2 MnCl_2 GIC, because of the same universality class. (i) The incommensurate short range spin order with nanoscale correlation is observed in the temperature range between 1.5 K and 15 K. (ii) The spin glass phase appears below T_{SG} ($= 10$ K). (iii) The magnetic specific heat shows no anomaly at T_{SG} . It shows double broad peaks at 13 and 80 K. (iv) The magnetic specific heat is proportional to T^2 in the low temperature side. (v) The entropy due to the broad peak around 13 K is 1/3 of the total entropy. It is surprising that in spite of difference in the detail of magnetic and structural parameters, the magnetic behavior of stage-2 MnCl_2 GIC is very similar to that of NiGa_2S_4 . This may imply that these common features are a key to understanding the physics of 2D XY -like or Heisenberg-like antiferromagnet on the triangular lattice.

II. EXPERIMENTAL PROCEDURE

The sample of stage-2 MnCl_2 GIC was prepared from kish graphite by vapor reaction of the powdered MnCl_2 in a chlorine-gas atmosphere of 740 Torr. The reaction was continued at 500°C for one month. The stoichiometry of the sample was determined from the weight-uptake measurement as $\text{C}_{12.70}\text{MnCl}_2$. The specific heat was measured by the thermal-relaxation method at low temperatures down to 0.4 K in magnetic fields parallel to the c plane up to 20 kOe on field cooling, using a commercial apparatus (PPMS, Quantum Design).

III. RESULT

A. Determination of nonmagnetic specific heat at $H = 0$

Figure 1 shows the T (temperature) dependence of specific heat (C) in zero field for a stage-2 MnCl_2 GIC based on single-crystal kish graphite, where the specific heat is expressed in the unit of $\text{J}/(\text{Mn mol K})$. The specific heat increases with increasing T at low temperatures below 5 K, becoming to flatten out between 5 K and 20 K, and it increases with further increasing T . There is no anomaly in C vs T around the spin freezing temperature T_{SG} ($= 1.1$ K), where the ZFC magnetization exhibits a relatively sharp peak.

In Figs. 2(a) and (b), we make a plot of C/T vs T^2 at $H = 0$ for stage-2 MnCl_2 GIC. It is found from Fig. 2

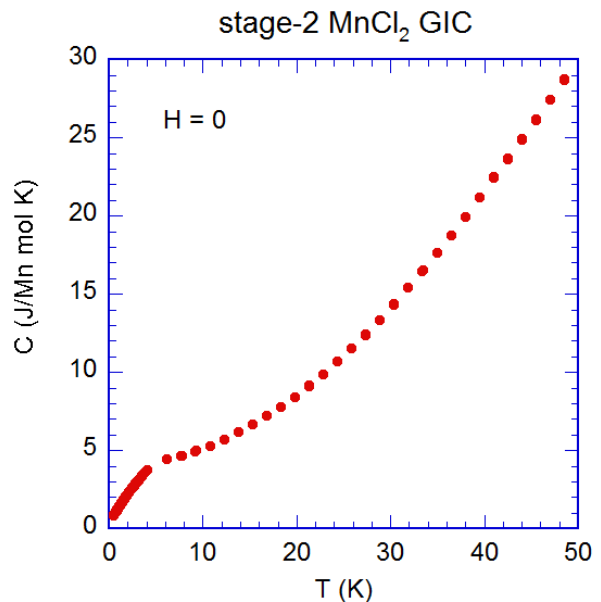


FIG. 1: (Color online) Plot of specific heat C in the units of $\text{J}/(\text{Mn mol K})$ vs T for stage-2 MnCl_2 GIC. $H = 0$. Note that two kinds of data which were separately taken under the same condition, are shown.

that C/T drastically decreases with increasing T^2 at low temperatures below 20 K. It shows a minimum around 20 K and in turn it increases with further increasing T^2 .

It is expected that the specific heat of stage-2 MnCl_2 GIC at low temperatures, C , is described by,

$$C = C_{mag} + C_{nonmag}, \quad (1)$$

with

$$C_{nonmag} = C_e + C_g = \gamma T + \beta T^3, \quad (2)$$

where C_e ($=\gamma T$) and C_g ($=\beta T^3$) represent the contributions of the conduction electrons and of the lattice to the specific heat, respectively, and C_{mag} is the magnetic contribution. Here we assume that the Deby temperature of stage-2 MnCl_2 GIC with stoichiometry $\text{C}_{12.70}\text{MnCl}_2$ is on the same order as that of the pristine graphite. Therefore the T^5 term of the C_{nonmag} may be negligibly small for $T < 50$ K. Then C/T is written as

$$\frac{C}{T} = \frac{C_{mag}}{T} + \frac{C_{nonmag}}{T} = \frac{C_{mag}}{T} + \gamma + \beta T^2. \quad (3)$$

In the temperature range where the magnetic contribution C_{mag}/T is negligibly small, the curve of C/T vs T^2 is a straight line with the y -intercept γ and the slope β .

In Fig. 2(a), we note that the data of C/T vs T^2 for $20 \leq T \leq 50$ K do not fall on a straight line, but is upward convex for any possible straight line corresponding to the plot of C_{nonmag}/T vs T^2 . This may imply that the magnetic specific heat might exhibit a small broad peak centered around 40 – 50 K. In fact the existence of

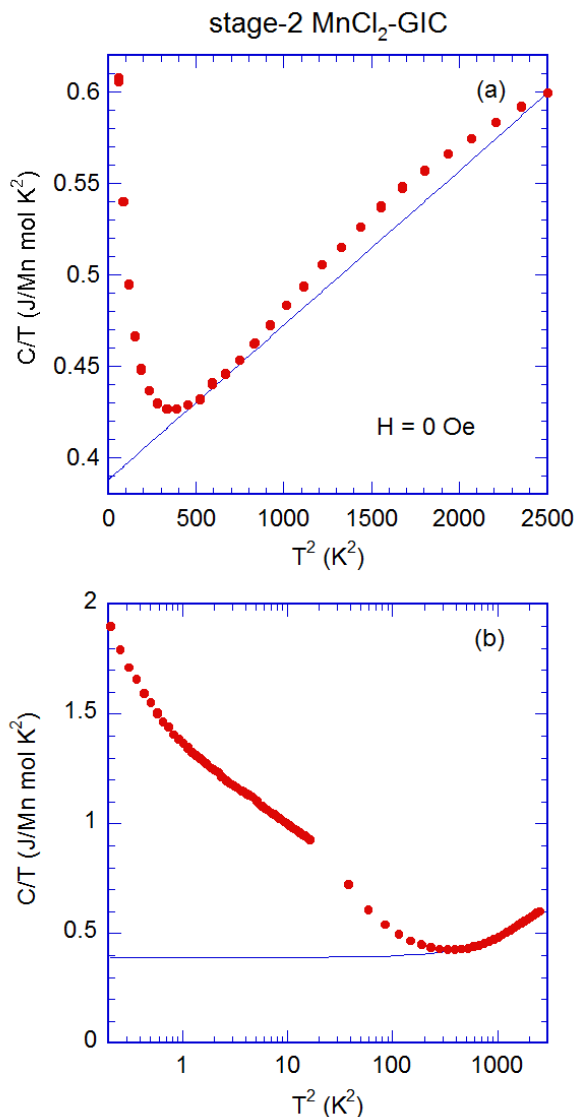


FIG. 2: (Color online)(a) C/T vs T^2 for stage-2 MnCl_2 GIC. $H = 0$. (b) Overview of the plot of C/T vs T^2 for stage-2 MnCl_2 GIC. $H = 0$. The solid line indicates the C_{nonmag}/T vs T^2 , which is obtained from the procedure described in the text.

the small broad peak has been confirmed from the AC calorimetry measurement by Koga and Suzuki.² Such a slight deviation of C/T vs T^2 for $20 \leq T \leq 50$ K from a straight line makes it difficult for one to determine exactly the T dependence of C_{nonmag} . Here we assume that the straight line for the plot C_{nonmag}/T vs T^2 passes two points at $T = 22.8$ K and 50.5 K. It is expressed by

$$\frac{C_{\text{nonmag}}}{T} = \gamma + \beta T^2, \quad (4)$$

with the parameters γ and β given by $\gamma = 0.38807$ (J/Mn mol K^2), and $\beta = 8.4397 \times 10^{-5}$ (J/Mn mol K^4). The advantage of the choice of the straight line for C_{nonmag}/T vs T^2 is that the plot of C/T vs T^2 is always above

the straight line for C_{nonmag}/T vs T^2 . In other words, C_{mag} is always positive. The disadvantage is that the T dependence of C_{mag} well above 20 K is rather sensitive to the choice of the straight line. Fortunately, the T dependence of C_{mag} well below 20 K, is not so sensitive to the choice of straight line, since the magnitude of C_{mag} is much larger than that of C_{nonmag} .

B. Magnetic specific heat C_{mag} vs T

In Fig. 3(a) we show the T dependence of C_{mag} for $H = 0$ at low temperatures, from the subtraction C_{nonmag} from C . Since C_{nonmag} is very small at low temperatures, the uncertainty of C_{mag} is negligibly small. The magnetic specific heat C_{mag} shows a broad peak around 5 K. No anomaly in C_{mag} vs T is observed at the spin freezing temperature T_{SG} ($= 1.1$ K). Above T_{cp} ($\simeq 5$ K), C_{mag} decreases as $1/T$ with increasing T . In Fig. 3(b) we show the T dependence of C_{mag} between 0.4 and 50 K. The magnetic specific heat exhibits a local minimum around 22 K, and a local maximum around 41 K. The peak height of C_{mag} around 41 K is dependent on the choice of C_{nonmag} as a background, since the contribution of C_{nonmag} to the specific heat C is large. The anomaly at 41 K is closely related to the change of the spin symmetry from isotropic to XY like. Wiesler et al.⁵ have reported the T dependence of the DC magnetic susceptibility (χ_{\perp} along the c plane and χ_{\parallel} along the c axis). Both χ_{\perp} and χ_{\parallel} decrease monotonically with increasing T and exhibits no anomaly around 50 K. Although $\chi_{\perp} > \chi_{\parallel}$ at all temperatures, the anisotropy $\Delta\chi = \chi_{\perp} - \chi_{\parallel}$ becomes appreciable only below 50 K. This may indicate the onset of short-range spin correlation in MnCl_2 layer.

C. T dependence of magnetic specific heat C_{mag} in the presence of H

Figure 4 shows the T dependence of the magnetic specific heat C_{mag} , where an external magnetic field H is applied along the c plane. The external magnetic field H is changed as a parameter; $H = 0, 2, 10,$ and 20 kOe. It is found that C_{mag} is strongly dependent on the magnetic field. As will be discussed in Sec. IV C, when the magnetic field is applied to our system at T below T_{SG} , the spin glass phase is destroyed and changes into the paramagnetic phase above the critical field $H_c(T)$. This is called the de Almeida-Thouless (AT) transition.¹⁷ The critical field $H_c(T = 0)$ (defined as H_{AT}) is evaluated as 5.87 ± 0.47 kOe. This implies that the system is at least in the spin glass phase at low fields ($H = 0,$ and 2 kOe).

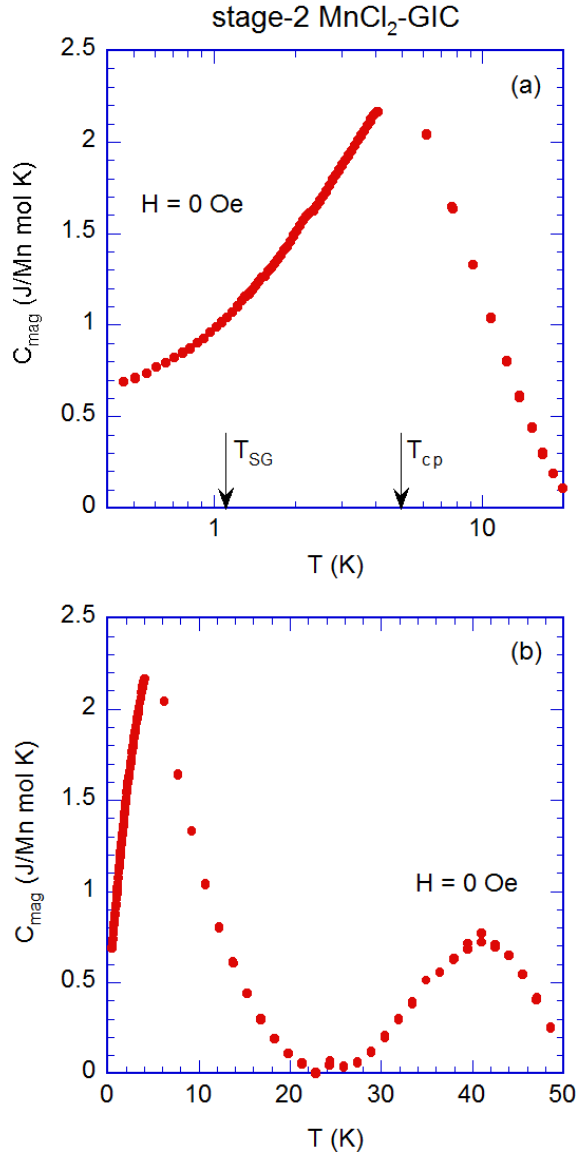


FIG. 3: (Color online) Plot of C_{mag} vs T for $T < 15$ K. C_{mag} shows a broad peak well above T_{SG} ($= 1.1$ K). C_{mag} exhibits no anomaly at $T = T_{SG}$, but exhibits a broad peak around T_{cp} (≈ 5 K). (b) Overview of the curve of C_{mag} vs T for $0 < T < 50$ K. C_{mag} shows double broad peaks around 5 and 41 K. The height of the peak around 41 K may be dependent on the choice of C_{nonmag} as a background. Since C_{nonmag} is very small at low temperatures below T_{SG} , the T dependence of C_{mag} is independent of the choice of C_{nonmag} .

D. T dependence of C_{mag} below T_{SG}

Figure 5 shows the plot of C_{mag}/T vs T for stage-2 $MnCl_2$ GIC at low temperatures below 4 K, where H is changed as a parameter. For $H = 0$ and 2 kOe, the curve of C_{mag}/T vs T drastically decreases with increasing T . For $H = 10$ kOe, it gradually decreases with increasing T . For $H = 20$ kOe, in contrast, the curve of C_{mag}/T vs

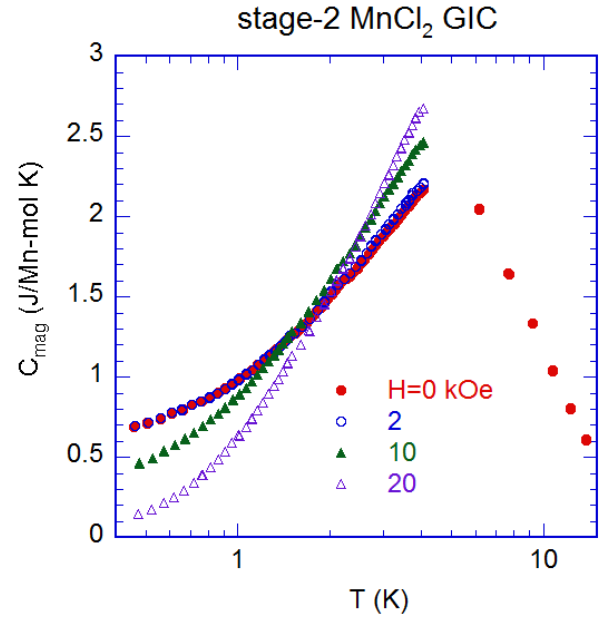


FIG. 4: (Color online) Magnetic specific heat C_{mag} vs T at low temperatures for stage-2 $MnCl_2$ GIC. An external magnetic field H is applied along the c plane (perpendicular to the c axis). $H = 0, 2, 10,$ and 20 kOe.

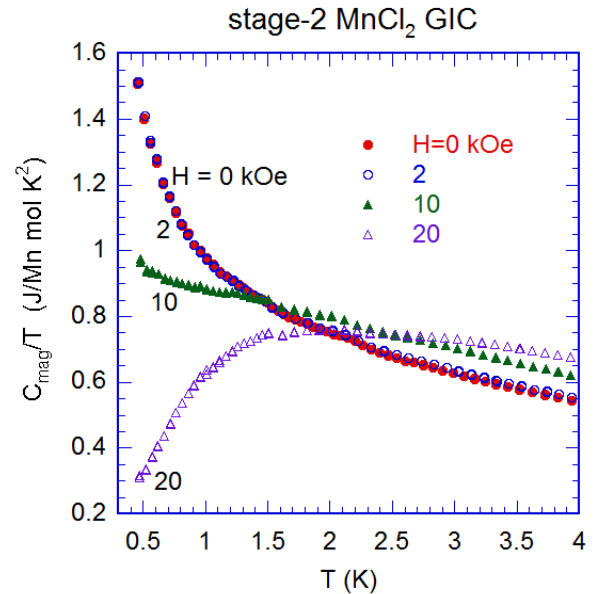


FIG. 5: (Color online) Plot of C_{mag}/T as a function of T where H is changed as a parameter. $H = 0, 2, 10,$ and 20 kOe. H is applied along the c plane.

T starts to increase linearly with increasing T and shows a broad peak around $T = 2$ K.

Here we examine the T dependence of C_{mag} below T_{SG} for each H . For $H = 20$ kOe, as shown in Fig. 6, the least-squares fit of the data of C_{mag}/T vs T for 0.45 K

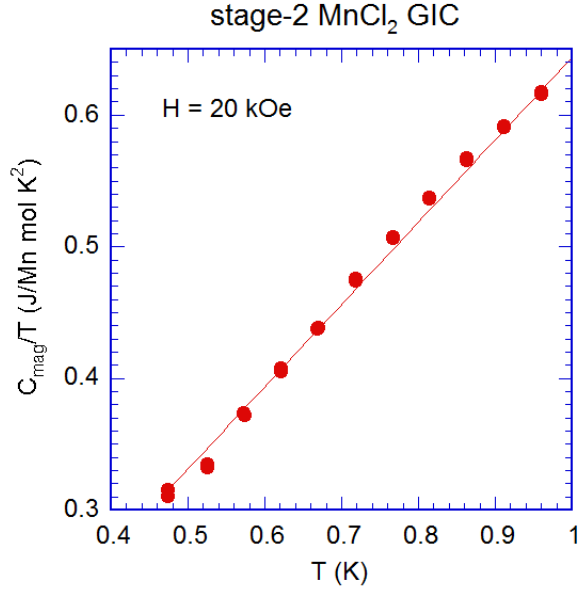


FIG. 6: (Color online) Plot of C_{mag}/T vs T for $H = 20$ kOe. C_{mag}/T is proportional to T below T_{SG} . The solid line is a least-squares fitting curve.

$\leq T \leq T_{SG}$ to

$$C_{mag}/T = \alpha_0 + \delta_0 T, \quad (5)$$

yields the parameters

$$\alpha_0 = 0.0186 \pm 0.0088 \text{ J/Mn mol K}^2$$

and

$$\delta_0 = 0.6253 \pm 0.0116 \text{ J/Mn mol K}^3.$$

This implies that the magnetic specific heat at $H = 20$ kOe is a sum of linear T dependence and the T^2 dependence below T_{SG} .

For $H = 10$ kOe, as shown in Fig. 7, C_{mag} is almost linearly proportional to T at low temperatures. The least-squares fit of the data of C_{mag} vs T at $H = 10$ kOe in the temperature range between 0.45 and 1.5 K to

$$C_{mag} = \alpha_1 + \delta_1 T, \quad (6)$$

yields the parameters

$$\alpha_1 = 0.077337 \pm 0.001986 \text{ J/Mn mol K}$$

and

$$\delta_1 = 0.80474 \pm 0.0019118 \text{ J/Mn mol K}^2.$$

We note that such a linear T dependence of C_{mag} at low temperatures is also observed in typical spin glasses such as $\text{Cu}_{0.988}\text{Mn}_{0.012}$ ¹⁸ and $\text{Eu}_{0.4}\text{Sr}_{0.6}\text{S}$.¹⁹ There are several models to explain the linear T dependence in spin glass. These models are discussed in detail by Fisher and

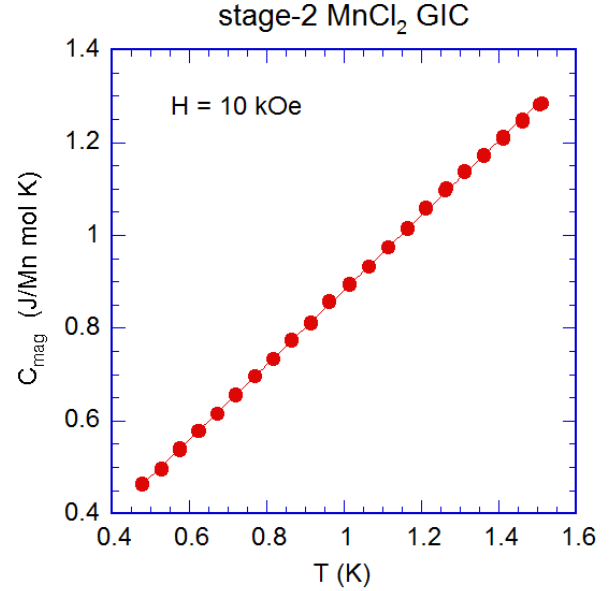


FIG. 7: (Color online) Plot of C_{mag} vs T for $H = 10$ kOe. The solid line is a best-fitting curve (straight line).

Herz.²⁰ A T^2 dependence of C_{mag} at low temperatures may indicate the presence of gapless and linearly dispersive modes in two dimensions. Such T^2 dependence of C_{mag} at low temperatures is observed in NiGa_2S_4 .¹⁴

For $H = 0$, as shown in Fig. 5, the upturn of the curve for C_{mag}/T vs T for $H = 0$ Oe is clearly seen in the low temperature ranges. Surprisingly, Wang and Swenson²¹ have predicted a peculiar property of the asymptotic low temperature specific heat,

$$C_{mag} = A \frac{1}{T^2} \exp\left(-\frac{\Delta}{T}\right), \quad (7)$$

or

$$\ln(C_{mag}T^2) = \ln(A) - \frac{\Delta}{T}, \quad (8)$$

using a replica Monte Carlo simulation method and finite-size transfer-matrix method for the 2D $\pm J$ Ising spin glass model, where A is constant and Δ is an energy gap between the ground state and the first excited state in spin glass phase. The validity of this form has been confirmed by Saul and Kardar,²¹ Lukic et al.,²³ and Katzbraber et al.,²⁴ in spite of the difference in the physical interpretation of Δ . The plot of $\ln(C_{mag}T^2)$ vs $1/T$ should be a straight line with a slope Δ .

Figure 8 shows the plot of $\ln(C_{mag}T^2)$ vs $1/T$ below T_{SG} for stage-2 MnCl_2 GIC at $H = 0$. It is found that the curve of $\ln(C_{mag}T^2)$ vs $1/T$ becomes a straight line for $0.45 < T < 0.7$ K, as shown in Fig. 8. The least-squares fit of these data to Eq.(8) yields the parameters

$$\Delta = 1.41 \pm 0.05 \text{ K}, \quad \ln(A) = 1.09 \pm 0.06.$$

The energy gap may disappear when the Zeeman energy ($g_{\perp}\mu_B SH$) as a result of the application of H to that system, becomes larger than the energy gap $k_B\Delta$, where S

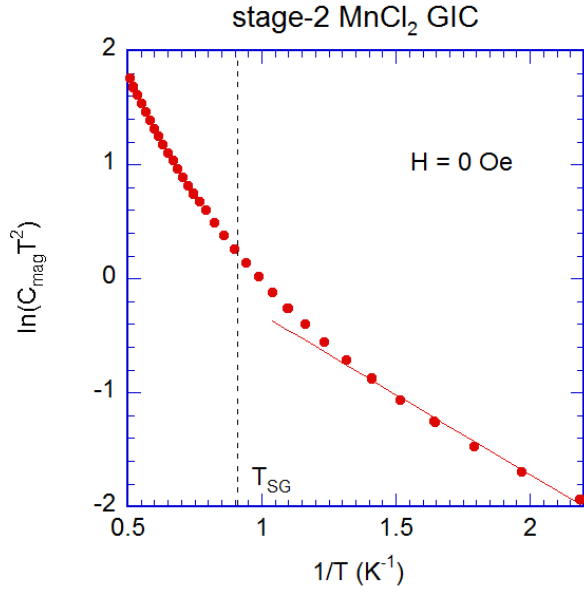


FIG. 8: (Color online) Plot of $\ln(C_{mag}T^2)$ vs $1/T$ at low temperatures for stage-2 MnCl_2 GIC. The straight line below T_{SG} is a least-squares fitting curve denoted by Eq.(8) with $\ln A = 1.0928$ and $\Delta = 1.407$ K.

= $5/2$ and $g_{\perp} = 1.977$. The critical magnetic field H_0 is evaluated as

$$H_0 \approx \frac{k_B \Delta}{g_{\perp} \mu_B S} = 4.25 \text{ kOe.}$$

The value of H_0 is on the same order as the critical magnetic field at $T = 0$ K for the AT transition;¹⁷ $H_{AT} = 5.87 \pm 0.47$ kOe.

E. Entropy vs T

Figure 9 shows the plot of entropy $\Delta S = S(T) - S(T_{min})$ as a function of T for stage-2 MnCl_2 GIC for $H = 0, 2, 10, 20$ kOe, where $T_{min} = 0.45$ K. The entropy ΔS is defined as

$$\Delta S = S(T) - S(T_{min}) = \int_{T_{min}}^T \frac{C(T')}{T'} dT'. \quad (9)$$

Since $S = 5/2$, the total entropy S_{total} is equal to

$$S_{total} = R \ln(2S + 1) = R \ln 6 = 14.898 \text{ J/Mn mol K,}$$

where R is the gas constant and $R = 8.314472$ J/Mn mol K. As shown in Fig. 9, the curve of ΔS vs T at $H = 0$ is upward convex, while the curve of ΔS vs T at $H = 20$ k Oe is downward convex. The curve of ΔS vs T at $H = 0$ is almost straight line, reflecting the linear T dependence of C_{mag} at $H = 10$ kOe. Figure 10 shows the T dependence of ΔS at $H = 0$ in the wide temperature

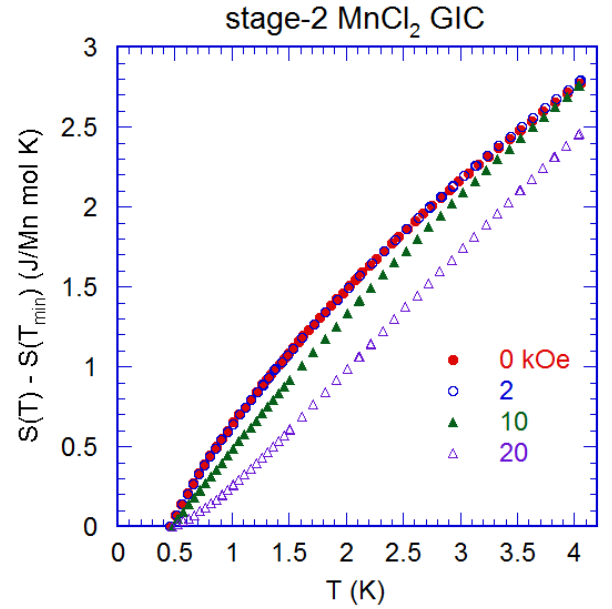


FIG. 9: (Color online) Entropy ($= S(T) - S(T_{min})$) vs T , which is calculated from the data of C_{max} vs T . $H = 0, 2$ kOe, 10 kOe, and 10 kOe. $T_{min} = 0.45$ K.

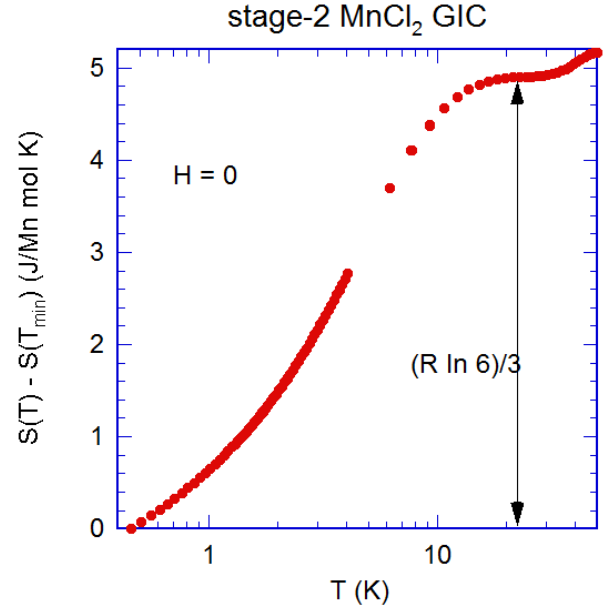


FIG. 10: (Color online) Overview of entropy ($= S(T) - S(T_{min})$) vs T , which is calculated from the data of C_{max} vs T . $H = 0$. $T_{min} = 0.45$ K. The entropy due to the broad peak around 5 K is $1/3$ of the total entropy.

region up to 50 K. The entropy ΔS becomes flat between 20 and 30 K. The value of ΔS at 20 K is nearly equal to $1/3$ of $R \ln 6$. This factor $1/3$ is also observed in the entropy in NiGa_2S_4 ,¹⁴ which may be feature common to the 2D AFT. There are two step-like changes around

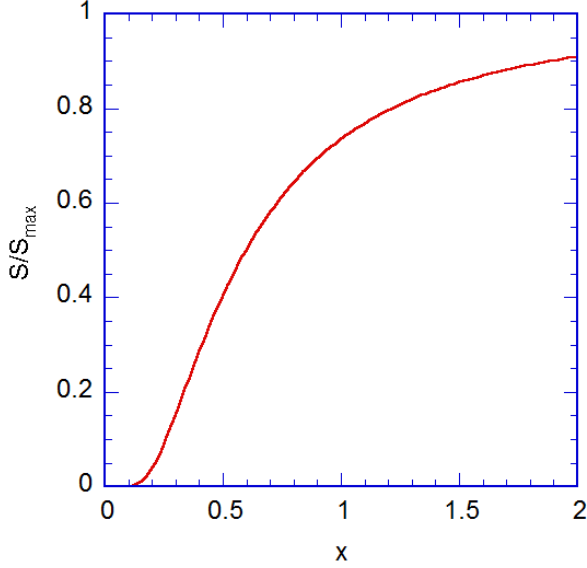


FIG. 11: (Color online) Normalized entropy given by S/S_{max} vs $x (= T/\Delta)$, where $S/S_{max} = f(x)$ defined by Eq.(11). $\Delta = 1.41$ K.

5 and 41 K corresponding to the peak temperatures of C_{mag} vs T . It is considered that there is small amount of entropy contributing to the total entropy above 50 K, because of the absence of anomaly in C_{mag} above 50 K.

We now evaluate the entropy $S(T)$ at low temperatures. To this end, we assume that C_{mag} is given by Eq.(7). Then the entropy is calculated as

$$\begin{aligned} S &= \int_0^T \frac{C}{T} dT = \int_0^T \frac{A}{T^3} \exp\left(-\frac{\Delta}{T}\right) dT \\ &= \frac{A}{T\Delta^2} (T + \Delta) \exp\left(-\frac{\Delta}{T}\right), \end{aligned} \quad (10)$$

leading to the scaling form of the entropy given by

$$\frac{S}{S_{max}} = f(x = \frac{T}{\Delta}) = \frac{(1+x) \exp(-\frac{1}{x})}{x}, \quad (11)$$

with $x = T/\Delta$ and $S_{max} = A/\Delta^2$ [=1.507 J/(Mn mol K)], where $f(x)$ is a scaling function of x . In Fig. 11, we show the plot of the normalized entropy S/S_{max} as a function of $x (= T/\Delta)$. As is clearly shown, the curve of S/S_{max} vs x is upward convex, which is similar to the the experimental curve of S vs T at $H = 0$ (see Fig. 9).

When $T_{min} = 0.45$ K and $\Delta = 1.41$ K, $S(T_{min})$ can be evaluated as $S(T_{min}) = 1.507f(x = T_{min}/\Delta) = 0.272$ J/Mn mol K from Fig. 11. Then the observed entropy at 50 K is calculated as

$$S(T = 50 \text{ K}) = S(T_{min}) + \Delta S = 5.47 \text{ J/Mn mol K}$$

This value of $S(T = 50 \text{ K})$ is much smaller than the total entropy (= 14.898 J/Mn mol K). The missing entropy

may be a residual entropy at $T = 0$ K because of highly frustrated nature of the system. This residual entropy is calculated as

$$S_{residual} \approx S_{total} - S(T = 50 \text{ K}) = 9.43 \text{ J/Mn mol K}$$

which corresponds to 63 % of the total entropy. The residual entropy occurs when the system can exist in a large number of ground states with the same zero-point energy. Note that for highly frustrated pyrochlore, $\text{Dy}_2\text{Ti}_2\text{O}_7$,²⁵ the residual entropy is 1/3 of the total entropy. Here we note that even the residual entropy is finite, still the magnetic specific heat is zero at $T = 0$ K,²⁶ since

$$\begin{aligned} S_{residual} &= \lim_{T \rightarrow 0} S = \lim_{T \rightarrow 0} \frac{TS}{T} = \lim_{T \rightarrow 0} (T \frac{dS}{dT} + S) \\ \lim_{T \rightarrow 0} C &= \lim_{T \rightarrow 0} T \frac{dS}{dT} = 0, \end{aligned} \quad (12)$$

IV. SUMMARY OF RESULTS FROM PREVIOUS WORKS AND FURTHER ANALYSIS

A. Magnetic neutron scattering

The MnCl_2 layer forms a triangular Mn^{2+} lattice in stage-2 MnCl_2 -GIC. Primitive lattice vectors \mathbf{a} and \mathbf{b} have length $|\mathbf{a}| = |\mathbf{b}| = 3.692 \pm 0.005 \text{ \AA}$, the same as for pristine MnCl_2 (3.693 \AA). The in-plane reciprocal lattice vector is given by \mathbf{a}^* and \mathbf{b}^* where $|\mathbf{a}^*| = |\mathbf{b}^*| = 4\pi/(\sqrt{3}a) = 1.965 \text{ \AA}^{-1}$. The magnetic neutron scattering results of stage-2 MnCl_2 GIC have been reported previously by Wiesler et al.^{8,9,10} The in-plane magnetic scattering at 0.43 K is obtained by subtracting the intensity at 14.85 K from the corresponding intensity at 0.43 K. Magnetic peaks are observed at $|\mathbf{Q}_\perp| = 0.522, 1.536, 2.05, \text{ and } 2.44 \text{ \AA}^{-1}$ (see Figs. 5 and 6 of Ref.¹⁰), where \mathbf{Q}_\perp is the in-plane wave vector. These wave vectors are consistent with the model shown in Fig. 12. According to this model, the magnetic Bragg reflections should appear at the in-plane wave vectors $\mathbf{Q}_\perp = \mathbf{G}(h, k) \pm \mathbf{k}_1$, $\mathbf{G}(h, k) \pm \mathbf{k}_2$, or $\mathbf{G}(h, k) \pm (\mathbf{k}_1 - \mathbf{k}_2)$, where $\mathbf{G}(h, k) = h\mathbf{a}^* + k\mathbf{b}^*$ is the in-plane reciprocal lattice vector of MnCl_2 layer, h and k are integers, and \mathbf{k}_i ($i = 1, 2$) are the reciprocal lattice vectors of magnetic superlattice. Assigning $|\mathbf{k}_1| = 0.522 \text{ \AA}^{-1}$ and $|\mathbf{a}^* - \mathbf{k}_1| = 1.536 \text{ \AA}^{-1}$, the angle θ between \mathbf{k}_1 and \mathbf{a}^* can be estimated as

$$\cos \theta = \frac{|\mathbf{a}^*|^2 + |\mathbf{k}_1|^2 - |\mathbf{a}^* - \mathbf{k}_1|^2}{2|\mathbf{k}_1||\mathbf{a}^*|}, \quad (13)$$

or $\theta = 30 \pm 2^\circ$. The magnetic Bragg reflections are predicted to occur at $|\mathbf{Q}_\perp| = |\mathbf{a}^* + \mathbf{k}_2| = 2.03 \text{ \AA}^{-1}$, and $|\mathbf{a}^* + \mathbf{k}_1| = 2.431 \text{ \AA}^{-1}$, in good agreement with the experimental values, $|\mathbf{Q}_\perp| = 2.05$ and 2.44 \AA^{-1} , respectively.

The temperature dependence of the scattering has been also studied by a series of in-plane scans at temperatures between 63 mK and 7.5 K. Throughout the entire

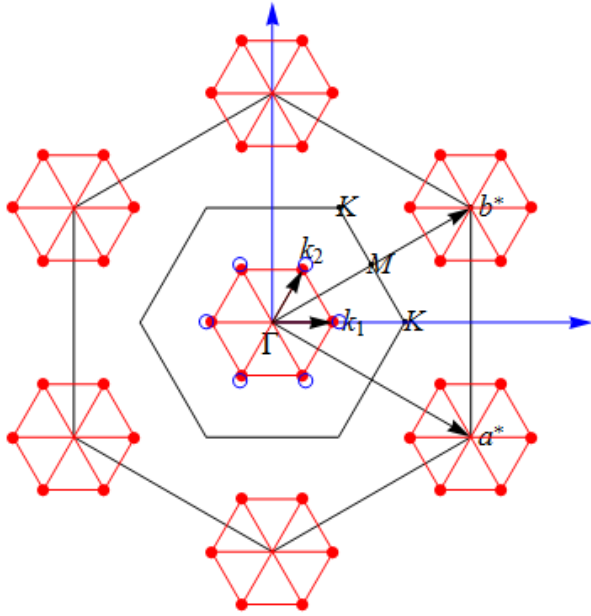


FIG. 12: (Color online) Magnetic Bragg reflections (denoted by solid circles) in the in-plane reciprocal lattice vector. $|\mathbf{a}^*| = |\mathbf{b}^*| = 1.965\text{\AA}^{-1}$. $|\mathbf{k}_1| = |\mathbf{k}_2| = 0.522\text{\AA}^{-1}$. The K point is denoted by $(\mathbf{a}^* + \mathbf{b}^*)/3$ or 120° spin structure or $\sqrt{3} \times \sqrt{3}$ spin structure; $|\mathbf{Q}_{com}| = \sqrt{3}|\mathbf{a}^*|/3 = 1.1345\text{\AA}^{-1}$. The points denoted by open circles correspond to the commensurate structure $2\sqrt{3} \times 2\sqrt{3}$ spin structure. These points are expressed by $(\mathbf{a}^* + \mathbf{b}^*)/6$; $|\mathbf{Q}_{com}| = \sqrt{3}|\mathbf{a}^*|/6 = 0.5672\text{\AA}^{-1}$. Note that the location of magnetic reflections is close to, but not equal to the magnetic Bragg reflections corresponding to the $2\sqrt{3} \times 2\sqrt{3}$ commensurate spin structure. The reciprocal lattice of the graphite layer is not included in this figure.

temperature range, the intensities fit well to a Lorentzian peak described by

$$I = \frac{I_0 \kappa}{\pi[(Q_\perp - \tau)^2 + \kappa^2]}, \quad (14)$$

around $|\mathbf{Q}_\perp| = |\mathbf{k}_1|$, where κ is the inverse in-plane spin correlation length, τ is the peak position, and I_0 is the integrated intensity. In Fig. 13 we show the T dependence of the peak position τ . The peak position τ is nearly constant at 0.522\AA^{-1} below 0.45 K and increases rapidly with increasing T in the vicinity of T_{SG} ($= 1.1$ K). Above T_{SG} , τ plateaus briefly at 0.532\AA^{-1} , rising again above 4.5 K (close to the peak temperature T_{cp} of C_{mag} vs T) toward the commensurate position at $|\mathbf{Q}_{com}| = \sqrt{3}|\mathbf{a}^*|/6 = 0.5672\text{\AA}^{-1}$ (see the original data of τ vs T in Fig. 7(a) in Ref.¹⁰), where $\mathbf{Q}_{com} = (\mathbf{a}^* + \mathbf{b}^*)/6$.

In Fig. 14 we show the T dependence of the inverse in-plane spin correlation length κ (see also the original data of κ vs T in Fig. 7(c) in Ref.¹⁰). The value of κ is 0.0566\AA^{-1} at 0.45 K, corresponding to an in-plane spin correlation length ξ ($= 1/\kappa$) of only 18\AA . The value of κ slowly increases with increasing T . It does not show any

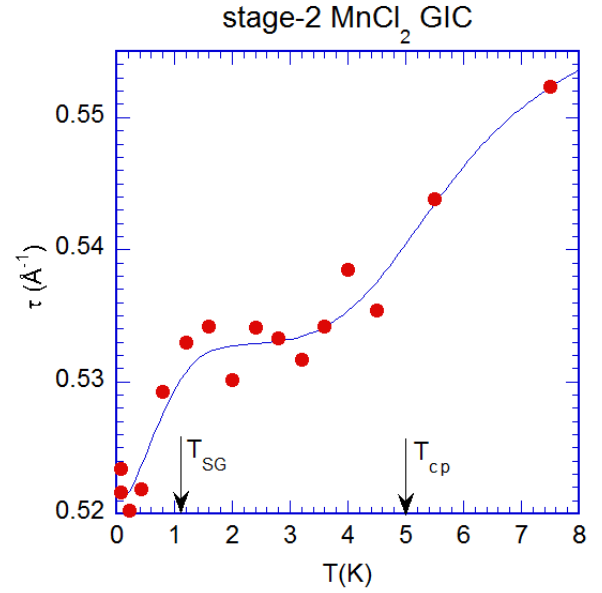


FIG. 13: (Color online) T dependence of the center of the Lorentzian peak, τ , for stage-2 MnCl_2 GIC. The original data of τ vs T were taken by Wiesler et al.¹⁰ $\tau = |\mathbf{Q}_{com}| = \sqrt{3}|\mathbf{a}^*|/6 = 0.5672\text{\AA}^{-1}$ corresponds to the commensurate in-plane spin structure with the periodicity $2\sqrt{3} \times 2\sqrt{3}$. The solid line is a guide to the eyes. $T_{SG} = 1.1$ K. $T_{cp} \simeq 5$ K.

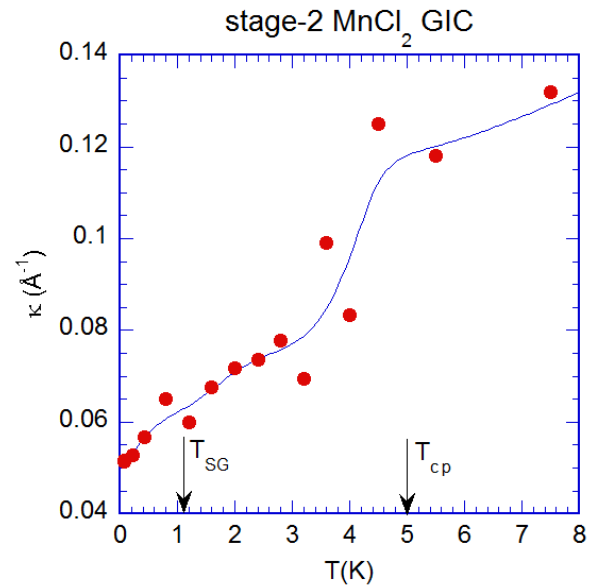


FIG. 14: (Color online) Inverse in-plane correlation length κ ($= 1/\xi$) vs T . ξ is the in-plane spin correlation length. The instrumental resolution limit for κ is 0.016\AA^{-1} . The original data of κ vs T were taken by Wiesler et al.¹⁰ The solid line is a guide to the eyes. $T_{SG} = 1.1$ K. $T_{cp} \simeq 5$ K.

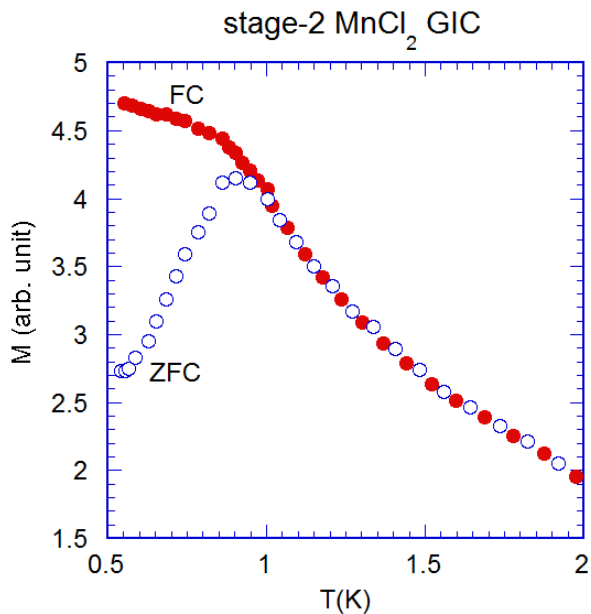


FIG. 15: (Color online) T dependence of M_{ZFC} and M_{FC} for stage-2 MnCl_2 GIC. See the detail of ZFC and FC cooling protocol in the text. The magnetization is measured at $H = 100$ mOe. The original data were taken by Matsuura et al.⁶

anomaly at T_{SG} . It undergoes a step-like change around 4.5 K, at which C_{mag} shows a broad peak. The value of κ is 0.124\AA^{-1} at 4.5 K, corresponding to an in-plane spin correlation length ξ of only 8\AA .

B. ZFC and FC magnetization

The T dependence of zero-field cooled (ZFC) magnetization and field-cooled (FC) magnetization for stage-2 MnCl_2 GIC has been reported by Matsuura et al.⁶ Their result is reproduced in Fig. 15. In the ZFC cooling protocol, the system is quenched from high temperatures well above T_{SG} down to 0.5 K in the absence of an external magnetic field. Then the external magnetic field ($H = 100$ mOe) is applied to the system at $T = 0.5$ K. The ZFC magnetization is measured with increasing T from 0.5 K to temperatures well above T_{SG} under the presence of H . The FC magnetization is measured with decreasing T from high temperatures well above T_{SG} down to 0.5 K, in the presence of H ($= 100$ mOe). The T dependence of M_{ZFC} and M_{FC} is very similar to that of typical spin glasses. M_{ZFC} shows a peak around $T = 0.9$ K. M_{ZFC} starts to deviate from M_{FC} below T_{SG} (≈ 1.0 K). In other words, the irreversible effect of magnetization occurs below T_{SG} . The value of T_{SG} thus determined from Fig. 15 is a little different from that of the AC magnetic susceptibility reported by Kimishima et al.^{3,4} Here we define that T_{SG} is equal to 1.1 K. The magnetization M_{FC} bends, becoming almost flat just below T_{SG} , which is one of the significant features of spin glasses. In

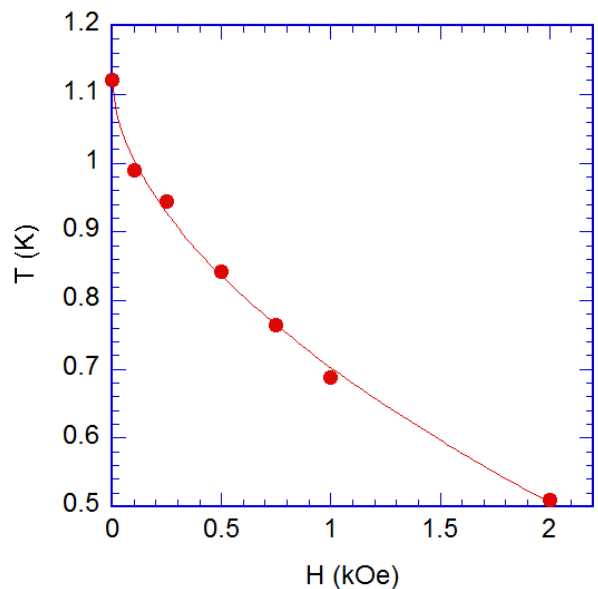


FIG. 16: (Color online) Plot of the peak temperature (χ' vs T in the presence of H) as a function of H for stage-2 MnCl_2 GIC. $H \parallel c$ plane. The original data were taken by Kimishima et al.^{3,4} The solid line is a best-fitting curve to Eq.(15).

summary, the stage-2 MnCl_2 GIC undergoes a spin glass phase transition at $T = T_{SG}$.

C. AC magnetic susceptibility, de Almeida-Thouless line

Kimishima et al.^{3,4} have reported the T dependence of AC magnetic susceptibility (the dispersion χ') for stage 2 MnCl_2 GIC in the presence of an external magnetic field H along the c plane. The dispersion χ' shows a peak at $T = T_{SG}$ ($= 1.1$ K). This peak shifts to the low temperature side with increasing H . In Fig. 16, we show the H dependence of the peak temperature for stage-2 MnCl_2 GIC which has been previously reported by Kimishima et al.⁴ It is predicted for typical spin glasses that the peak temperature $T_{SG}(H)$ forms a de-Almeida-Thouless (AT)¹⁷ line in the H - T magnetic phase diagram, which is defined by

$$H = H_{AT} \left[1 - \frac{T_{SG}(H)}{T_{SG}(H=0)} \right]^p, \quad (15)$$

where p is an exponent and $p = 3/2$, and H_{AT} is the magnetic field at $T = 0$ K. The least-squares-fit of the data of $T_{SG}(H)$ vs H to Eq.(15) yields the parameters

$$T_{SG}(H=0) = 1.184 \pm 0.013 \text{ K},$$

$$p = 1.79 \pm 0.10, \text{ and } H_{AT} = 5.87 \pm 0.47 \text{ kOe}.$$

The exponent p thus obtained is relatively close to $p = 3/2$ for the AT line. This indicates that the low temperature phase below T_{SG} is a spin glass phase. Here

we note that the characteristic field H_{AT} is theoretically predicted as (Katori and Ito)²⁷

$$H_{AT} = \sqrt{\frac{8}{(m+1)(m+2)} \frac{k_B T_{SG}(H=0)}{g\mu_B S}}, \quad (16)$$

where $m = 1$ for the Ising symmetry and $m = 3$ for the Heisenberg symmetry, g is the Landé g -factor, k_B is the Boltzmann constant, and μ_B is the Bohr magneton. The value of H_{AT} is evaluated as 2.103 kOe for $m = 1$ and as 3.839 kOe for $m = 3$, where $g = g_{\perp} = 1.97$ for stage-2 MnCl_2 GIC. These values of H_{AT} is smaller than the derived from the analysis of the least-squares fitting.

D. DC magnetic susceptibility

The DC magnetic susceptibility of stage-2 MnCl_2 GIC has been reported by Wiesler et al.⁵ The parameters of the magnetic properties are listed in Table I. Both χ_{\parallel} and χ_{\perp} (measured in the FC state) decrease monotonically with increasing T and exhibits no anomaly around 41 K, where the magnetic specific heat C_{mag} shows a broad peak. $\chi_{\perp} > \chi_{\parallel}$ at all temperatures, which suggests that spins align in the MnCl_2 layer. The anisotropy $\Delta\chi = \chi_{\perp} - \chi_{\parallel}$ becomes appreciable only below 50 K, a result with a shift of the g -values below 50 K, may indicate that onset of short-range spin order with $\mathbf{Q} = 0$ mode in the MnCl_2 layer.

As listed in Table I, the Curie-Weiss temperature Θ_{\perp} along the c plane is equal to -9.1 K, and the Curie-Weiss temperature Θ_{\parallel} along the c axis is equal to -5.9 K. The negative sign of Θ_{\perp} and Θ_{\parallel} indicates that the intraplanar exchange interaction is antiferromagnetic. The peak temperature ($T_{cp} \simeq 5$ K) of C_{mag} vs T is on the same order as $|\Theta_{\parallel}|$ and $|\Theta_{\perp}|$.

E. Line width of electron spin resonance

The electron spin resonance (ESR) of stage-2 MnCl_2 GIC has been measured by Koga and Suzuki,² and Suzuki et al.⁷ Figure 17 shows the T dependence of ESR linewidth ΔH for stage-2 MnCl_2 GIC when the external magnetic field H is applied along the c axis (\parallel). The line width ΔH is defined as the peak-to-peak width of the derivative ESR line shape.

The T dependence of ΔH_{\parallel} for $H \parallel c$ is consistent with that of $T\chi_{\parallel}$ for $6 \leq T \leq 20$ K. This suggests that the $\mathbf{Q} = 0$ mode is dominant in these temperature ranges. As T decreases from 6 K ($\approx |\Theta_{\parallel}| = 5.9$ K), the mode $\mathbf{Q} = \mathbf{Q}_{incomm}$ of the spin fluctuations takes over the $\mathbf{Q} = 0$ mode, where \mathbf{Q}_{incomm} is the wave vector corresponding to the in-plane incommensurate spin structure (close to the $2\sqrt{3} \times 2\sqrt{3}$ spin structure). The minimum of ΔH_{\parallel} around 6 K results from the competition between the $\mathbf{Q} = 0$ mode and $\mathbf{Q} = \mathbf{Q}_{incomm}$ mode. The magnitude

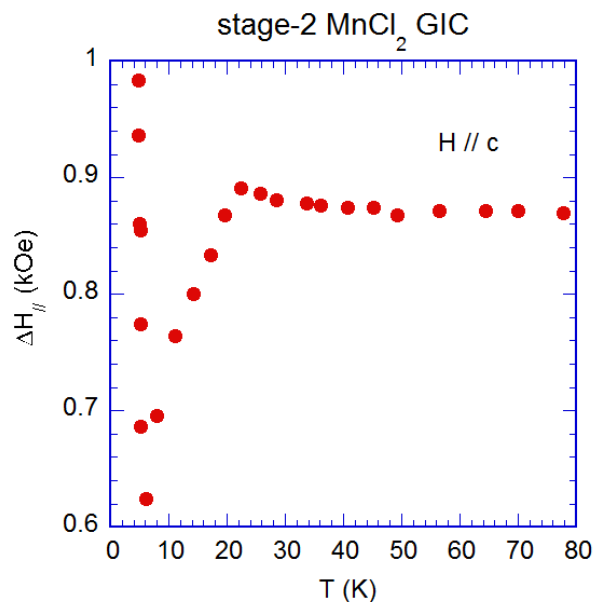


FIG. 17: (Color online) T dependence of the ESR line-width ΔH for stage-2 MnCl_2 GIC. $H \parallel c$. The ESR measurement was made by the conventional field-modulated X-band spectrometer at frequency $\nu = 9.42$ GHz in the temperature range between 1.38 and 293 K. The original data were taken by Koga and Suzuki,² Suzuki et al.⁸

τ ($= |\mathbf{Q}_{incomm}|$) decreases with decreasing T as is observed from the magnetic neutron measurements. The linewidth ΔH_{\parallel} diverges as T approaches T_{SG} from the high temperature side.

V. DISCUSSION

A. Nature of short range spin order in the vicinity of T_{SG}

The origin of the incommensurate in-plane short range spin order is discussed, based on the model proposed by Sakakibara²⁸ who explains the magnetic structure of C_6Eu (donor-type stage-1 GIC), where C_6Eu has a hexagonal closed packed (hcp) type structure. Here we assume that stage-2 MnCl_2 GIC also have the hcp type structure, which is schematically shown in Fig. 18. For simplicity, only the positions of Mn^{2+} ions are shown. From the symmetry of the stacking sequence in hcp-type structure, we assume that there are two kinds of stacking sequences such as $ABABAB$ (Fig. 18) and $ACACAC \dots$ in the weight of 1 to 1, where A , B , and C layers forms a triangular lattice. The positions of Mn^{2+} ions in the B and C layers are shifted by the translation vectors Δ and 2Δ with respect to those of atoms in the A layer, where

$$\Delta = \frac{1}{3}(2\mathbf{a} + \mathbf{b}).$$

TABLE I: Parameters of the structure and magnetism in stage-2 MnCl_2 GIC.^{3,4,5,6,7,8,9,10}

| parameter | value | description |
|-----------------------------------|---------------------------|---|
| $ \mathbf{a}^* = \mathbf{b}^* $ | 1.965 \AA^{-1} | in-plane reciprocal lattice of MnCl_2 layer |
| $ \mathbf{Q}_{comm} $ | 0.5672 \AA^{-1} | wave number for the $2\sqrt{3} \times 2\sqrt{3}$ spin structure |
| $ \mathbf{Q}_{incomm} $ | 0.522 \AA^{-1} | wave number for the incommensurate short range spin order at 0.45 K |
| a | 3.692 \AA | in-plane lattice constant of MnCl_2 layer |
| d | 12.80 \AA | c -axis repeat distance |
| Θ_{\perp} | -9.1 K | Curie-Weiss temperature along the c plane |
| Θ_{\parallel} | -5.9 K | Curie-Weiss temperature along the c axis |
| P_{\perp} | $5.831 \mu_B$ | effective magnetic moment along the c plane |
| P_{\parallel} | $5.838 \mu_B$ | effective magnetic moment along the c axis |
| g_{\perp} | 1.977 | g -factor along the c plane at room temperature |
| g_{\parallel} | 1.912 | g -factor along the c axis at room temperature |
| J_1 | -0.20 K | antiferromagnetic n.n. intraplanar exchange interaction |
| D | 0.97 K | positive single ion anisotropy, showing XY symmetry |
| T_{SG} | 1.1 K | spin freezing temperature |
| S | $5/2$ | spin of Mn^{2+} |

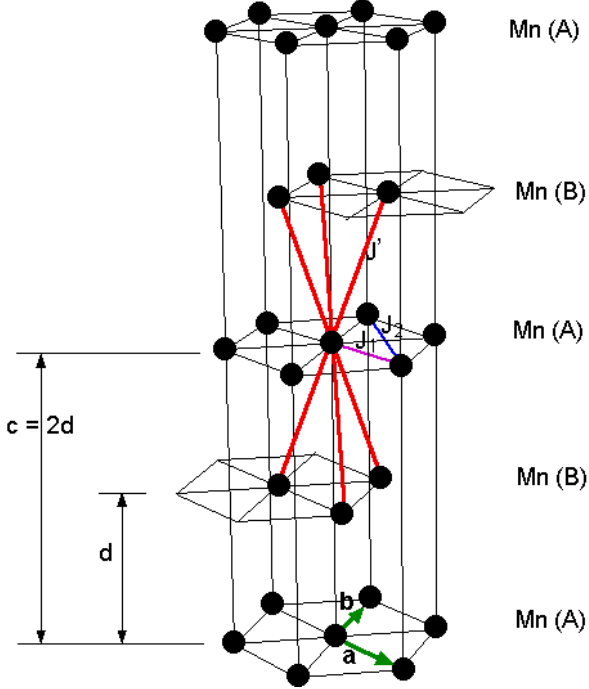


FIG. 18: (Color online) Simplified model for the hexagonal-closed packed (hcp) type structure of stage-2 MnCl_2 GIC, where only the positions of Mn^{2+} ions are shown. $a = 3.692 \text{ \AA}$. $d = 12.80 \text{ \AA}$. \mathbf{a} , \mathbf{b} and \mathbf{c} are lattice vectors.

The lattice vectors are described in terms of the Cartesian coordinates, as

$$\mathbf{a} = \left(\frac{1}{2}a, -\frac{\sqrt{3}}{2}a, 0 \right), \mathbf{b} = \left(\frac{1}{2}a, \frac{\sqrt{3}}{2}a, 0 \right), \mathbf{c} = (0, 0, 2d).$$

where a is the lattice constant ($= 3.692 \text{ \AA}$), d is the c -axis repeat distance ($d = 12.80 \text{ \AA}$), and $c = 2d$ is the lattice constant along the c axis. The reciprocal lattice vectors are also described in terms of the Cartesian coordinates, as

$$\mathbf{a}^* = \frac{4\pi}{\sqrt{3}a} \left(\frac{\sqrt{3}}{2}, -\frac{1}{2}, 0 \right), \mathbf{b}^* = \frac{4\pi}{\sqrt{3}a} \left(\frac{\sqrt{3}}{2}, \frac{1}{2}, 0 \right),$$

$$\mathbf{c}^* = \frac{2\pi}{2d} (0, 0, 1).$$

where $a^* = |\mathbf{a}^*| = 4\pi/(\sqrt{3}a)$ and $c^* = |\mathbf{c}^*| = \pi/d$. The K point in the Brillouin zone (see Fig. 12) is expressed by

$$\frac{1}{3}(\mathbf{a}^* + \mathbf{b}^*) = \frac{4\pi}{3a} (1, 0, 0) = a^* \frac{1}{\sqrt{3}} (1, 0, 0).$$

The reciprocal vectors \mathbf{a}^* and \mathbf{b}^* are denoted in Fig. 12, where the K point is on the Q_x axis. According to Sakakibara,²⁸ the minimum energy of the system is given by

$$E_{\min} = -NS^2 J(\mathbf{Q}), \quad (17)$$

with

$$J(\mathbf{Q}) = \sum_{\mathbf{R}_{ij}} J(\mathbf{R}_{ij}) e^{i\mathbf{Q} \cdot \mathbf{R}_{ij}}, \quad (18)$$

where \mathbf{Q} is the characteristic wave vector, the N is total number of Mn^{2+} ions, \mathbf{S}_i is the classical spin vector of Mn^{2+} ion at the \mathbf{R}_i site, $\mathbf{R}_{ij} = \mathbf{R}_i - \mathbf{R}_j$, $J(\mathbf{R}_{ij})$ is the exchange interaction between \mathbf{S}_i at the \mathbf{R}_i site and \mathbf{S}_j at \mathbf{R}_j site: $J(\mathbf{R}_{ij}) = J(-\mathbf{R}_{ij})$. In our system, $J(\mathbf{Q})$ is defined by

$$J(\mathbf{Q}) \equiv J_1(\mathbf{Q}) + J_2(\mathbf{Q}) + J_3(\mathbf{Q}) + J'(\mathbf{Q}), \quad (19)$$

with

$$J_1(\mathbf{Q}) = 2J_1[\cos(aQ_x) + 2\cos(\frac{aQ_x}{2})\cos(\frac{\sqrt{3}}{2}aQ_y)], \quad (20)$$

$$J_2(\mathbf{Q}) = 2J_2[\cos(\sqrt{3}aQ_y) + 2\cos(\frac{3}{2}aQ_x)\cos(\frac{\sqrt{3}}{2}aQ_y)], \quad (21)$$

$$J_3(\mathbf{Q}) = 2J_3[\cos(2aQ_x) + 2\cos(aQ_x)\cos(\sqrt{3}aQ_y)], \quad (22)$$

$$J_4(\mathbf{Q}) = 2J' \cos(dQ_z)[2\cos(\frac{aQ_x}{2})\cos(\frac{aQ_y}{2\sqrt{3}}) + \cos(\frac{aQ_y}{\sqrt{3}})], \quad (23)$$

where J_1 is the nearest neighbor (n.n.) intraplanar exchange interaction (antiferromagnetic in the present system), J_2 is the next-nearest neighbor (n.n.n.) intraplanar exchange interaction, J_3 is the next next-nearest neighbor (n.n.n.n.) intraplanar exchange interaction, and J' is the interplanar exchange interaction. The wavenumbers Q_x , Q_y , and Q_z are defined as

$$Q_x = \frac{4\pi}{\sqrt{3}a}h = a^*h, Q_y = \frac{4\pi}{\sqrt{3}a}k = a^*k, Q_z = \frac{\pi}{d}\zeta = c^*\zeta.$$

The in-plane spin structure is realized as a result of the minimum energy state with a characteristic in-plane wave vector \mathbf{Q} , as

$$\mathbf{S}_i = S \cos(\mathbf{Q} \cdot \mathbf{R}_i)\mathbf{e}_x + S \sin(\mathbf{Q} \cdot \mathbf{R}_i)\mathbf{e}_y, \quad (24)$$

on the triangular lattice site \mathbf{R}_i ,

We need to find the location of the magnetic Bragg points in the \mathbf{Q} space for each pair of J_1 , J_2 , J_3 , and J' . The magnetic Bragg reflection appears at the vector \mathbf{Q} , where $J(\mathbf{Q})$ has a maximum. To this end, we use a ContourPlot (equi-energy contour plot) of $J(\mathbf{Q})$ in the Mathematica, where the points with the same $J(\mathbf{Q})$ are connected, forming an contour line. When $J_1 = -1$ (for simplicity the magnitude is normalized as 1, antiferromagnetic), $J_2 = J_3 = J' = 0$, the magnetic Bragg points appear at the K point, $(1/3\mathbf{a}^* + 1/3\mathbf{b}^*)$. The in-plane spin structure with \mathbf{Q} at the K point is a 120° spin structure ($\sqrt{3} \times \sqrt{3}$) as is expected.

We determine the magnetic phase diagram in the (J_2, J_4) plane where $J_1 = -1$ and $J_3 = 0$. The magnetic phase diagram consists of the K point reflection ($\sqrt{3} \times \sqrt{3}$), the M point reflection (2×2), and ($\sqrt{7} \times \sqrt{7}$) reflections, depending on the values of J_2 and J_4 . The detail of the magnetic phase diagram will be reported elsewhere. In the limited case of $J_1 = -1$, $-0.02 \leq J_2 \leq 0.08$, and $J' = 2$, the magnetic Bragg points appear at the point $(\mathbf{a}^*/6 + \mathbf{b}^*/6)$, or $Q_x = ha^*$ and $Q_y = ka^*$ with $h = \sqrt{3}/6 = 0.28675$ and $k = 0$. In Figs. 19(a) and (b), we show the energy-contour plot of $J(\mathbf{Q})$, where $J_1 = -1$, $J_2 = 0$, and $J' = 2$. It is clear that $J(\mathbf{Q})$ has a maximum at $h = 0.28675$ and $k = 0$, which is the Bragg peak from the commensurate in-plane spin structure. Note that the energy contour plot of Fig. 19(b) is similar to the schematic diagram of the reciprocal lattice phase shown in Fig. 12.

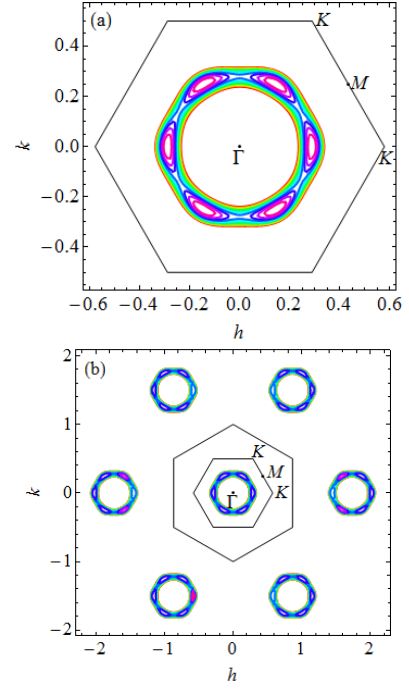


FIG. 19: (Color online) Energy contour line of $J(\mathbf{Q})$ for $J_1 = -1$, $J_2 = 0$, $J_3 = 0$, and $J' = 2$ in the (h, k) plane. $Q_x = a^*h$, $Q_y = a^*k$, $Q_z = 0$. $h = 0.28675$ and $k = 0$ for the $|\mathbf{Q}_{comm}| = 0.5672\text{\AA}^{-1}$.

Because of $J' > 0$, J' is a ferromagnetic interplanar interaction. The magnitude of J' is larger than that of J_1 . This result seems to be inconsistent with our assumption that $|J'|$ is much smaller than $|J_1|$. However, if the effective interplanar exchange interaction J'_{eff} is used instead of J' and the magnitude of J'_{eff} becomes large with decreasing T , the above inconsistency may be ruled out. Below 30 K where the static magnetic susceptibility becomes anisotropic, the short-range spin order gradually grows with decreasing T . This growth leads to the effective interplanar exchange interaction between adjacent MnCl_2 layers,

$$J'_{eff} = J'(\xi_{\perp}/a)^2, \quad (25)$$

with $\xi_{\perp} = 18\text{\AA}$ at 0.45 K and $a = 3.692\text{\AA}$. Even if $|J'|$ is very small, the effective interaction $|J'_{eff}|$ becomes large when ξ_{\perp} become large with decreasing T . Then $|J'_{eff}|$ gives rise to a spin correlation between Mn^{2+} ions of adjacent MnCl_2 layers.

In the present stage, we cannot find any appropriate values of (J_2, J_4) for the magnetic Bragg peak at the incommensurate spin structure ($h = 0.2656$, $k = 0$) corresponding to $|\mathbf{Q}_{incomm}| = 0.522\text{\AA}^{-1}$ from our method. Note that this situation may change when J_3 is taken into account.

Using Eq.(24), the in-plane spin structure with a characteristic \mathbf{Q} can be obtained on the triangular lattice without knowing the values of J_1 , J_2 , J_3 , and J' . Fig-

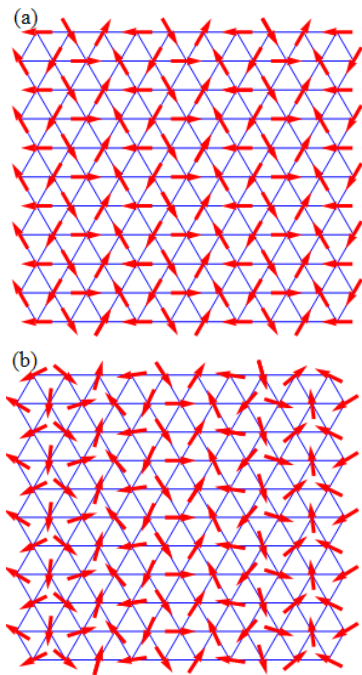


FIG. 20: (Color online) (a) Commensurate in-plane spin structure with $|\mathbf{Q}_{comm}| = 0.5672\text{\AA}^{-1}$. $2\sqrt{3} \times 2\sqrt{3}$ spin structure. (b) Incommensurate in-plane spin structure with $|\mathbf{Q}_{incomm}| = 0.522\text{\AA}^{-1}$.

ure 20(a) and (b) shows the commensurate in-plane spin structures with $|\mathbf{Q}_{comm}| = 0.5672\text{\AA}^{-1}$, and incommensurate in-plane spin structure with $|\mathbf{Q}_{incomm}| = 0.522\text{\AA}^{-1}$.

B. Nature of reentrant spin glass phase

Below T_{SG} , the short range in-plane spin order characterized by the incommensurate in-plane wavevector $\tau = |\mathbf{Q}_{incomm}|$ coexists with the spin glass phase. The in-plane correlation length slightly increases from 17\AA at T_{SG} to 18\AA ($\approx 5a$) at 0.45 K with decreasing T . The wavevector $\tau = |\mathbf{Q}_{incomm}|$ decreases from 0.535\AA^{-1} at T_{SG} to 0.522\AA^{-1} at 0.45 K with decreasing T , where $|\mathbf{Q}_{comm}| = 0.5672\text{\AA}^{-1}$. This means that the degree of the incommensurability of in-plane spin order with the Mn lattice is slightly enhanced well below T_{SG} . The in-plane spin correlation length almost remains unchanged below T_{SG} partly because of the highly geometrically frustrated-nature of the 2D AFT.

The spin glass phase observed in our system is rather different from that of the dilute Ising antiferromagnet $\text{Fe}_{0.55}\text{Mg}_{0.45}\text{Cl}_2$. Wong et al.²⁹ have shown that the spin glass behavior and the long-range antiferromagnetic (AF) order coexist in the low temperature phase, forming the reentrant spin glass phase (RSG). The system undergoes

magnetic phase transitions at the Néel temperature $T_N = 7.5\text{ K}$ and the reentrant spin glass transition temperature $T_{RSG} = 3.0\text{ K}$. The AF phase with long range spin order exists between T_N and T_{RSG} and the RSG phase exists below T_{RSG} . The AF order is long range ($> 10^3\text{\AA}$) both between T_N and T_{RSG} , and below T_{RSG} . In other words, it is unaffected by the reentrant spin glass transition. The microscopic picture of the coexistence may consist of spins in an infinite AF network and spins frozen like spin glass. In our system, there are two kinds of spins, spins in the short range spin order and the frustrated spins. The spin direction of the frustrated spins are frozen below T_{SG} because of the spin frustration effect arising from the competing interactions. The short range spin order is not destroyed since this spin order is already established well above T_{SG} .

VI. CONCLUSION

The magnetic properties of stage-2 MnCl_2 GIC are discussed in terms of the experimental results of specific heat as well as ZFC and FC magnetization, AC magnetic susceptibility, magnetic neutron scattering, and ESR. The short range spin order with associated with the incommensurate wave vector $|\mathbf{Q}_{incomm}|$ ($= 0.522\text{\AA}^{-1}$ at 0.45 K) appears below 5 K ($\approx |\Theta_{\perp}|, |\Theta_{\parallel}|$), where the magnetic specific heat C_{mag} has a broad peak. The wavevector $|\mathbf{Q}_{incomm}|$ is close to the wavevector ($|\mathbf{Q}_{comm}| = \sqrt{3}|\mathbf{a}^*|/6 = 0.5672\text{\AA}^{-1}$) of the commensurate in-plane spin structure with $(2\sqrt{3} \times 2\sqrt{3})$ periodicity. The in-plane spin correlation length slightly increases with decreasing T and reaches only 18\AA at 0.45 K below T_{SG} . In the low temperature phase below T_{SG} , the spin glass phase coexists with the short-range spin order associated with the incommensurate wave vector $|\mathbf{Q}_{incomm}|$. The residual entropy at 0 K is estimated to be 63 % of the total entropy because of highly frustrated nature of the system. The entropy due to the broad peak around 5 K is 1/3 of the total entropy. The temperature ($= 41\text{ K}$) at which C_{mag} shows a broad peak is the onset temperature of short-range spin order. These features are common to the systems with the same universality class, 2D XY antiferromagnet on the triangular lattice.

Acknowledgments

We are grateful to Prof.M. Matsuura, Prof. Y. Kimishima, Dr. D.G. Wiesler, Dr. N. Rosov and Dr. K. Koga for invaluable discussions during their collaborations on the study on the magnetic properties of stage-2 MnCl_2 GIC since 1980's. The specific heat measurement was done at Tohoku University.

- * suzuki@binghamton.edu
† itsuko@binghamton.edu
- ¹ T. Enoki, M. Suzuki, and M. Endo, *Graphite Intercalation Compounds and Applications* (Oxford University Press, New York, 2003).
 - ² K. Koga and M. Suzuki, *J. Phys. Soc. Jpn.* **53**, 786 (1984).
 - ³ Y. Kimishima, A. Furukawa, H. Nagano, P.C. Chow, D.G. Wiesler, H. Zabel, and M. Suzuki, *Synthetic Metals* **12**, 455 (1985).
 - ⁴ Y. Kimishima, A. Furukawa, M. Suzuki, and H. Nagano, *J. Phys. C: Solid State Phys.* **19**, L43 (1986).
 - ⁵ D.G. Wiesler, M. Suzuki, P.C. Chow, and H. Zabel, *Phys. Rev. B* **34**, 7951 (1986).
 - ⁶ M. Matsuura, Y. Karaki, T. Yonezawa, and M. Suzuki, *Jpn. J. Appl. Phys.* **26**, Supplement **26-3** (1987) 773.
 - ⁷ M. Suzuki, S.M. Sampere, and K. Koga, *Phys. Rev. B* **39**, 6979 (1989).
 - ⁸ D.G. Wiesler, M. Suzuki, I.S. Suzuki, and N. Rosov, *Phys. Rev. Lett.* **75**, 942 (1995).
 - ⁹ M. Suzuki, I.S. Suzuki, D.G. Wiesler, and N. Rosov, *J. Phys. Chem. Solids* **57**, 729 (1996).
 - ¹⁰ D.G. Wiesler, M. Suzuki, I.S. Suzuki, and N. Rosov, *Phys. Rev. B* **55**, 6382 (1997).
 - ¹¹ S. Miyashita and H. Shiba, *J. Phys. Soc. Jpn.* **53**, 1145 (1984).
 - ¹² H. Kawamura, and S. Miyashita, *J. Phys. Soc. Jpn.* **53**, 4138 (1984).
 - ¹³ D.H. Lee, R.G. Caflish, J.D. Joannopoulos, and F.Y. Wu, *Phys. Rev. B* **29**, 2680 (1984).
 - ¹⁴ S. Nakatsuji, Y. Nambu, H. Tonomura, O. Sakai, S. Jonas, C. Broholm, H. Tsunetsugu, Y. Qiu, and Y. Maeno, *Science* **309**, 1697 (2005). S. Nakatsuji, Y. Nambu, K. Onuma, S. Jonas, C. Broholm, and Y. Maeno, *J. Phys. Condens. Matter* **19**, 145232 (2007).
 - ¹⁵ H. Takeya, K. Ishida, K. Kitagawa, Y. Ihara, K. Onuma, Y. Maeno, Y. Nambu, S. Nakatsuji, D.E. MacLaughlin, A. Koda, and R. Kadono, *Phys. Rev. B* **77**, 054429 (2008).
 - ¹⁶ D. E. MacLaughlin, Y. Nambu, S. Nakatsuji, R. H. Heffner, Lei Shu, O. O. Bernal, and K. Ishida, *Phys. Rev. B* **78**, 220403 (R) (2008).
 - ¹⁷ J.R.J. de Almeida and D.J. Thouless, *J. Phys. A Math. Gen.* **11**, 983 (1978).
 - ¹⁸ L.E. Wenger and P.H. Keesom, *Phys. Rev. B* **13**, 4053 (1976).
 - ¹⁹ D. Meschede, F. Steglich, W. Felsch, H. Maletta, and W. Zinn, *Phys. Rev. Lett.* **44**, 102 (1980).
 - ²⁰ K.H. Fischer and J.A. Hertz, *Spin Glasses* (Cambridge University Press, Cambridge, 1991).
 - ²¹ J. Wang and R. H. Swendsen, *Phys. Rev. B* **38**, 4840 (1988).
 - ²² L. Saul and M. Kardar, *Phys. Rev. E* **48**, R3221 (1993).
 - ²³ J. Lukic, A. Galluccio, E. Marinari, O.C. Martin, and G. Rinaldi, *Phys. Rev. Lett.* **92**, 11720 (2004).
 - ²⁴ H G. Katzgraber, L. W. Lee, and I. A. Campbell, arXiv: cond-mat/0510668v1 (2005).
 - ²⁵ A. P. Ramirez, A. Hayashi, R. J. Cava, R. Siddharthan, and B. S. Shastry, *Nature* **399**, 333 (1999).
 - ²⁶ R. Kubo, in *Physics in Random Systems*, edited by T. Yonezawa, R. Abe, T. Oguchi, and T. Haseda, Chapter 15 *Statistical Physics of Random Systems* (Baifukan, Tokyo, 1981) [in Japanese].
 - ²⁷ H. Aruga Katori and A. Ito, *J. Phys. Soc. Jpn.* **63**, 3122 (1994).
 - ²⁸ T. Sakakibara, *J. Phys. Soc. Jpn.* **53**, 3607 (1984).
 - ²⁹ Po-zen Wong, S.von Molnar, T.T.M. Palstra, J.A. Mydosh, H. Yoshizawa, S.M. Shapiro, and A. Ito, *Phys. Rev. Lett.* **55**, 2043 (1985).